

## X-ray-absorption spectroscopic studies of sodium polyphosphate glasses

Zhanfeng Yin, Masoud Kasrai,\* and G. Michael Bancroft

*Department of Chemistry, University of Western Ontario, London, Ontario, Canada N6A 5B7*

Kim H. Tan and Xinghong Feng

*Canadian Synchrotron Radiation Facility, University of Wisconsin, Stoughton, Wisconsin 53589*

(Received 21 June 1994)

A series of sodium polyphosphate glasses of composition  $\text{Na}_{n+2}\text{P}_n\text{O}_{3n+1}$  have been studied using synchrotron-radiation x-ray-absorption spectroscopy. High-resolution P *L*-edge and *K*-edge x-ray appearance near-edge structure (XANES) as well as *K*-edge extended x-ray-absorption fine structure (EXAFS) of the phosphates have been investigated. It has been found that while the *K*-edge XANES spectra of different phosphate glasses are similar, the *L*-edge XANES features are strikingly different. These results show that the intensities of the low-energy spin-orbit doublet in the P *L*-edge spectra increase with average chain length of polyphosphate glasses. The increase is very rapid up to  $n = 20$ , then it levels off as the chain length increases above this value. Using this information, a quantitative calibration curve has been established which can be used to determine the chain length of polyphosphates in bulk or surface films. The features observed in the XANES spectra of the polyphosphates have been assigned. From EXAFS measurements, the average bond distances and coordination numbers around P have been measured. It was found that within the accuracy of EXAFS, average P-O bond distances in polyphosphate glasses do not change substantially.

### INTRODUCTION

Amorphous phosphates have been studied for over 100 years. In 1816, Berzelius<sup>1</sup> found that, when ordinary phosphoric acid is ignited, the product is fundamentally different from orthophosphoric acid in that it acquires the power of coagulating a solution of albumen. However, it was not until the middle of the 20th century that the problem of the number and kind of condensed phosphates was solved in general. One of the main reasons for this was that no analytical techniques were available for adequately differentiating between the various condensed phosphates. With the advancement in structural chemistry, attempts were made to investigate the structures of phosphates. By sharing oxygen atoms between tetrahedra, branched polymers of interconnected  $\text{PO}_4$  tetrahedra (chains or rings) can be produced.<sup>2</sup>

Phosphate glasses have gained increasing interest because of their low transformation temperatures and relatively high thermal-expansion coefficients compared with their silicate counterparts.<sup>3</sup> Phosphates have been widely used in surface coating materials<sup>4</sup> and safe immobilization and disposal of high-level nuclear wastes.<sup>5</sup> Recently they have been used as superionic glasses<sup>6</sup> and molded lenses in optical applications.<sup>7</sup> The interest in phosphates has also been intensified in parallel with progress in biological materials. For example, calcium phosphate based glasses are quite promising for application in artificial bone and tooth materials.<sup>8-11</sup> Such growing technological importance has, therefore, led to an increasing need for better understanding of amorphous phosphates and their properties.

In response to these requirements, several techniques have been used to analyze the structures and polymeriza-

tion of amorphous phosphates. They include x-ray<sup>12</sup> and neutron-diffraction studies,<sup>13</sup> infrared,<sup>14</sup> Raman,<sup>14(a),15</sup> optical-absorption<sup>16</sup> and electron-paramagnetic-resonance<sup>17</sup> spectroscopies. Recently high-performance liquid chromatography has been used to determine the phosphate chain length for short and intermediate chain lengths.<sup>14(b),15</sup> Nuclear magnetic resonance has been widely utilized to study the different chemical environments of phosphorus in phosphates such as the terminal phosphate groups, the middle group and the branching group.<sup>7(a),18</sup> X-ray photoelectron spectroscopy<sup>7(b),19,20</sup> (XPS) utilizing O (*1s*) and P (*2p* and *2s*) has been used to determine the percentage of  $\text{Na}_2\text{O}$  in phosphates. It has been found that a linear relationship exist between an extra peak in the O *1s* region and the amount of oxygen in the phosphate.

Limited applications of extended x-ray-absorption fine-structure (EXAFS) spectroscopy to the cation in phosphates have been reported in the literature.<sup>21</sup> However, no systematic study on the P *L* and *K* edges has been undertaken. In this paper, x-ray-absorption spectroscopies (EXAFS and XANES) at the P *K*-edge and *L*-edge have been used to investigate the chemical structures of a series of phosphate glasses. To our knowledge, this is the first time that the P *L*-edge XANES spectroscopy of the polyphosphate glasses have been reported. The intensities of pre-edge structures has been used to determine the chain length of these polyphosphate glasses.

### EXPERIMENT

#### Sample preparation

Sodium salt of polyphosphate glasses were purchased from the Sigma company. The average chain lengths of

polyphosphates reported by the company have been determined by end group titration.<sup>22</sup> Other phosphates were purchased from the Aldrich company and used without further purification. The samples were ground to a fine powder and pressed lightly on a Cu conducting tape. All the experiments were conducted in vacuum.

#### Data acquisition and analysis

Phosphorus x-ray-absorption spectra were obtained at the Canadian Synchrotron Radiation Facility<sup>23</sup> situated at the 1-GeV Aladdin storage ring, University of Wisconsin, Madison. For the *K*-edge spectra, the double-crystal monochromator (DCM) beamline which covers the energy region of 1500–4000 eV was used. For the *L*-edge spectra, the Grasshopper beamline, in which the x-ray beam is monochromatized by an 1800 g/mm grating and covers the photon region of 70–900 eV, was used. The photon resolutions at the DCM and Grasshopper are 1.0 and 0.2 eV, respectively, at the phosphorous *K*-edge and *L*-edge energy regions. The photoabsorption spectra were recorded in the total electron yield (TEY) and fluorescence yield (FY) modes using a microchannel plate.<sup>24</sup> The FY and TEY spectra for the P *L*-edge were very similar but because the FY spectra give slightly better resolution, only the FY spectra will be presented in this paper. For the *K* edge, no gain in resolution was obtained using FY. Thus TEY spectra, which give a stronger signal, will be presented. The energy scale for the DCM was calibrated setting the strong absorption line (white line) of elemental sulphur at 2472.0 eV, and

that of the Grasshopper was calibrated with reference to the lowest pre-edge peak of elemental sulphur at 162.7 eV. These values are not absolute values, but are close to the binding energy of S 1s and S 2p levels, respectively. The relative energy scale was reproducible within  $\pm 0.05$  eV. For the *L*-edge spectra a single scan, with good signal-to-noise ratio could be accomplished in  $\sim 5$  min. However, in most cases at least three scans were digitally combined and after normalization, a background was removed.

#### RESULTS AND DISCUSSIONS

X-ray-absorption spectroscopy, in general, deals with the transition of electrons from an atomic core level to unoccupied states in gases, liquids, and solids. The theory and principles of this technique has been covered extensively.<sup>25,26</sup> The technique has flourished with the advent of synchrotron radiation as a powerful x-ray source. Using monochromatized synchrotron radiation, it is possible to tune the x-ray energies to probe the atomic species in which the excitation occurs. In the last decade, the technique has been widely used for structure determination in complex biological, chemical, and surface systems. In this study, both P *L*-edge and *K*-edge x-ray-absorption spectra have been investigated for a series of phosphate and polyphosphate compounds.

#### Comparison of P *K*-edge and *L*-edge XANES spectra

The near-edge structure in an absorption spectrum covers a range from  $\sim 5$  eV below to  $\sim 50$  eV above the threshold. In Fig. 1 phosphorus *K*-edge (left) and *L*-edge

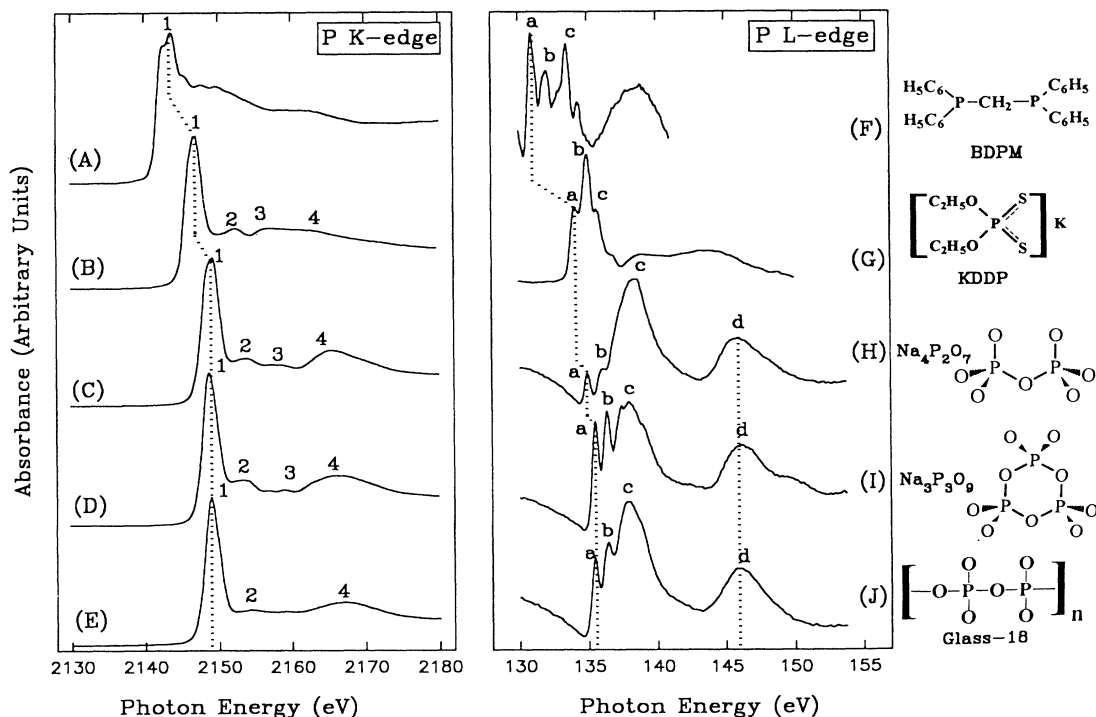


FIG. 1. P *K*-edge (left) and *L*-edge (right) XANES spectra of model compounds.

(right) XANES spectra of several phosphorus compounds including polyphosphates are compared. The structures of bis(diphenylphosphino) methane (BDPM), potassium diethyldithiophosphate (KDDP), and three phosphates are shown in the figure. It is obvious from the figure that the edge jumps in both *K* edge and *L* edge have shifted from BDPM to phosphates. The same shifts are generally observed for other elements, such as silicon<sup>27</sup> and sulphur.<sup>28,29</sup> The reason for this shift is due to the higher electronegativity of oxygen compared with sulphur and carbon. Therefore in phosphate, inner-shell electrons are less screened and thus more tightly bound which results in a higher chemical shift.

First we consider the *K*-edge spectra in Fig. 1 (left). All phosphate *K*-edge spectra recorded are similar to the two spectra shown in Fig. 1. They consist of one sharp transition [peak 1 in (C)–(E)] arising from an electron transition from the 1*s* core level to the  $t_2^*$  (*p*-like) antibonding orbital, and several relatively weaker peaks (peak 2,3,4) that most likely correspond to shape resonances or multiple scattering.<sup>30</sup> Features in *K*-edge spectra of glasses resemble that of the crystalline phosphates. As can be seen from Fig. 1, peaks 2, 3, 4 in glasses are weaker than those in phosphates and peak 4 is shifted to high energy by 1–2 eV. This pattern did not extend to long chain phosphate glasses, and basically the spectra of Glass-5 (*n* = 5) to Glass-44 (*n* = 44) looked very similar. Therefore, the *K*-edge XANES spectra of higher chain lengths will not be presented.

In contrast, *P L*-edge spectra are more complex and hence yield more information than their *K*-edge counterparts. The photon resolution and natural linewidth are more favorable at the *P L* edge than the *K* edge. For example, in the *K*-edge spectra, the linewidth of peak 1 is greater than 2 eV, and the difference between Na<sub>4</sub>P<sub>2</sub>O<sub>7</sub> (C) and Na<sub>3</sub>P<sub>3</sub>O<sub>9</sub> (D) spectra is very small. The relative intensities of peaks 2 and 3 changed only slightly. In contrast, the linewidth of peaks *a* and *b* in the *L*-edge spectra are ~0.6 eV, and the spectra of the phosphates are quite different. For example, the intensities of peaks *a* and *b* in Na<sub>4</sub>P<sub>2</sub>O<sub>7</sub> (H) are much lower than those in Na<sub>3</sub>P<sub>3</sub>O<sub>9</sub> (I). The intensities of peaks *a* and *b* in the polyphosphate glass spectra (*J*) are also quite different from the two crystalline compounds.

#### Peak assignment of *P L*-edge spectra

In silicon and sulphur *L*-edge x-ray-absorption spectroscopic studies,<sup>27,31</sup> the lowest spin-orbit doublet (*a* and *b*) has been assigned to the  $2p_{3/2,1/2} \rightarrow a_1^*$  transitions. Peak *b* is separated by 0.8–0.9 eV from *a*, which indicates that peak (*b*) is the spin-orbit counterpart of peak (*a*); the spin-orbit separation is 0.86 eV.<sup>32</sup> But the relative intensity of (*a*) and (*b*) is not what is generally found in XPS studies. This observation is not uncommon in photoabsorption spectroscopy<sup>33,34</sup> and has been discussed by Schwarz.<sup>35</sup> This assignment is also in agreement with the systematic study of the oxides and oxyanions of the third-row elements.<sup>27</sup> It has been shown that for SiO<sub>2</sub>, PO<sub>4</sub><sup>3-</sup>, SO<sub>4</sub><sup>2-</sup>, and ClO<sub>4</sub><sup>-</sup>, the first peak (doublet) in *L*-edge spectra is due to the transition of the  $2p$  electron to the

$a_1^*$  molecular orbital. The change in intensity of the doublet (peaks *a* and *b*) in Figs. 1(H), 1(I), and 1(J) is likely due to the distortion of the phosphate tetrahedra.

The assignment of peak *c* is still controversial. Previously it has been assigned to the electron transition to a mixed-valence band.<sup>31</sup> People seldom considered it a *p*-like transition because it is forbidden. However, recently Hansen, Brydson, and McComb<sup>36</sup> have shown that this peak for SiO<sub>2</sub> is due to the transition to a *p*-like  $t_2^*$  orbital. This arises because of significant mixing of *p* and *d* atomic orbitals. The assignment is also in agreement with Dehmer's results.<sup>37</sup>

Peak *d* is usually assigned to *d*-like shape resonances.<sup>27,36,37</sup> From spectra (H)–(J) in Fig. 1 we notice that this peak is always present at the same energy position for all phosphates, whether crystalline or glassy. However, when oxygen is replaced for other elements with lower electronegativity, the peak is shifted to lower energies.<sup>38</sup>

#### Polyphosphate glasses and *P L*-edge XANES spectroscopy

In 1950, Van Wazer and Holst found that the branching or cross-linked phosphates are relatively less stable than linear or cyclic structures.<sup>39</sup> This conclusion is called the antibranching rule and originally stems from x-ray and pH titration data. This has also been supported by hydrolytic degradation experiments<sup>40–43</sup> and thermodynamic analysis.<sup>44</sup> Thus according to the antibranching rule, the phosphate glasses that have been obtained commercially for this study have long chain structures. Because of the mutual repulsion exerted by the negative phosphate charges, ring structures are not as favorable.<sup>45</sup> Phosphate glass is a very special and interesting material in which the units are arranged one dimensionally in space, but are irregularly oriented. The general formula of chain phosphates can be expressed as  $M_{n+2}P_nO_{3n+1}$ , where *n* is the number of phosphorus and *M* is a univalent metal. The average chain length or average degree of polymerization  $\bar{n}$  of these anions is given by the following equation:<sup>46</sup>

$$\bar{n} = \frac{2}{R-1}, \quad (1)$$

where *R* is the molecular ratio of univalent cation to phosphorus in a given phosphate. It has been demonstrated in both amorphous and crystalline systems that the  $M_2O:P_2O_5$  ratio of a system is a dominant controlling factor. For any single molecule the ratio precisely dictates the chain length.<sup>46</sup> Figure 2 shows that as *n* (proportional to chain length) increases,  $1/R (= P/M)$  ratio increases. The increase is very sharp up to  $n \approx 20$  and then it levels off and approaches unity.

To further investigate the relationship between the *P L*-edge XANES spectra and polyphosphate properties, the spectra of a series of phosphates and polyphosphate glasses with different chain lengths have been measured. These are the only well characterized commercially available polyphosphates. However, recently we have synthesized a series of zinc polyphosphates. The characteris-

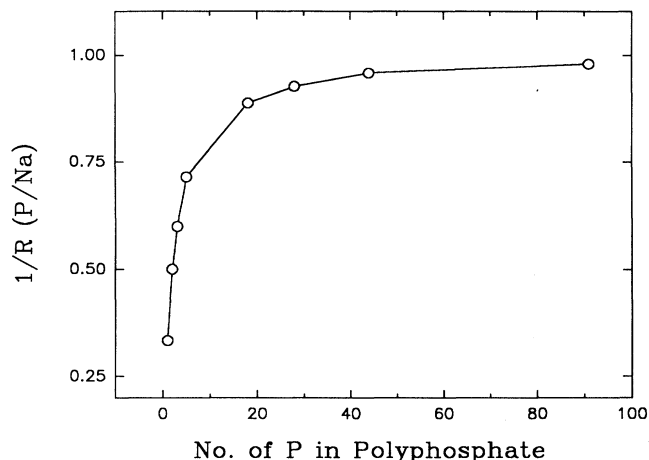


FIG. 2. Number of P in polyphosphates (chain length) versus the ratio of P to Na.

tics of zinc polyphosphates glasses, which turned out to be very similar to the sodium glasses, will be reported elsewhere.<sup>47</sup>

The P *L*-edge XANES spectra of sodium phosphates are shown in Figs. 3 and 4. Except for sodium orthophosphate ( $\text{Na}_3\text{PO}_4$ ), sodium pyrophosphate ( $\text{Na}_4\text{P}_2\text{O}_7$ ),

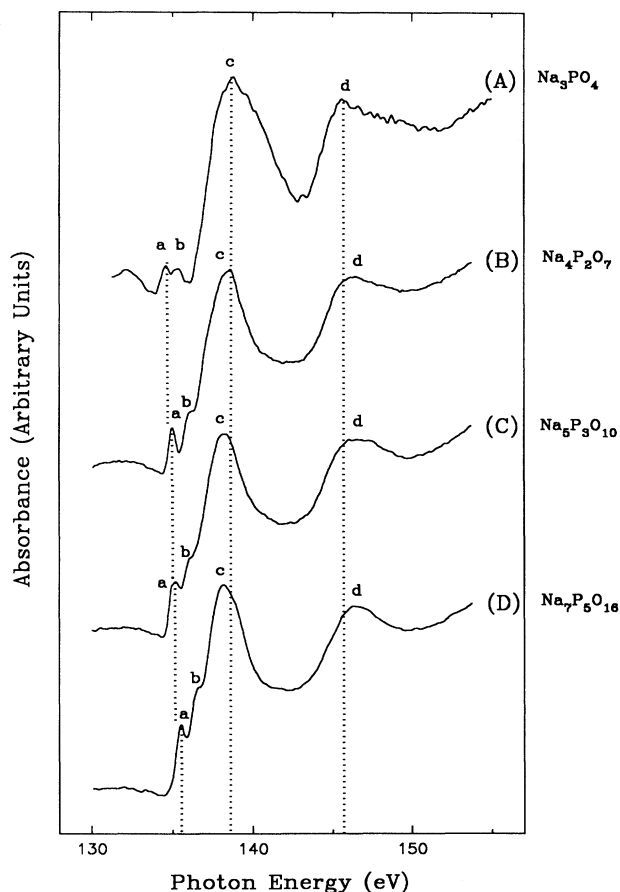


FIG. 3. P *L*-edge XANES spectra of the series of polyphosphates:  $n = 1-5$ .

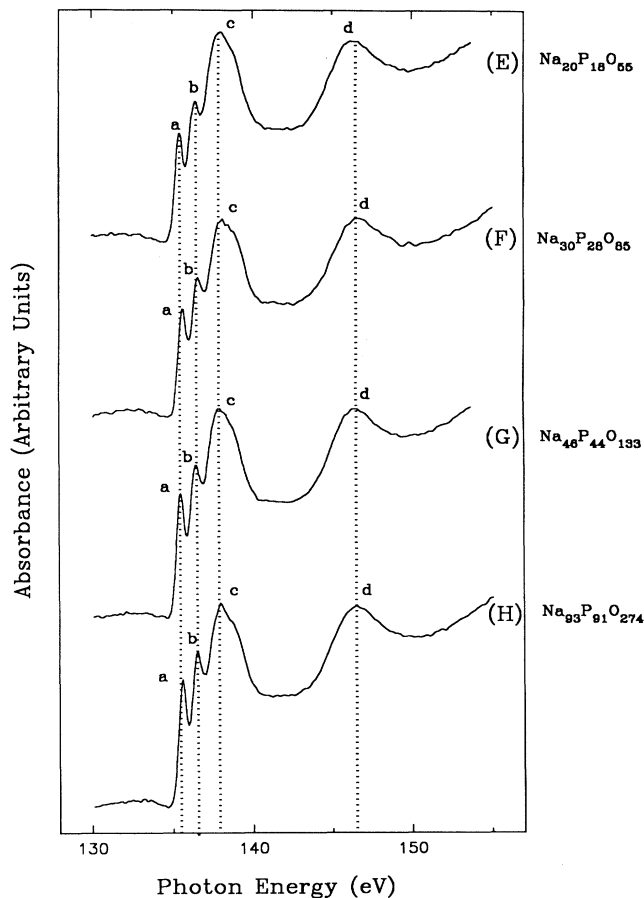


FIG. 4. P *L*-edge XANES spectra of the series of polyphosphates:  $n = 18-91$ .

pentasodium tripolyphosphate ( $\text{Na}_5\text{P}_3\text{O}_{10}$ ), and sodium metaphosphate ( $\text{Na}_3\text{P}_3\text{O}_9$ ) which are in crystalline forms, the rest of phosphates were glass. All phosphates shown in the figures are sodium salts, which makes their spectra comparable. Spectrum (A) of orthophosphate is the only one with peaks *a* and *b* well resolved from peak *c* due to larger separation between the doublet and peak *c* (see Table I). Spectra (D)–(H) are phosphate glasses with the number of phosphorus in the chain varying from 5 to 91. As can be noticed, peak *a* shifts to high energy from orthophosphate ( $n = 1$ ) to Glass-5 ( $n = 5$ ).

Most strikingly, it is obvious from Figs. 3 and 4 that the relative intensities of peaks *a* and *b* are very sensitive to the number of P in the linear polyphosphate glasses. In order to obtain accurate peak positions, peak widths and peak intensities for polyphosphate glasses, all the spectra were fitted to Gaussian lines using a least-squares program.<sup>28</sup> As illustrated by Fig. 5, the spectra of phosphates have been fitted to several Gaussian peaks representing the transition of P *2p* electrons to the  $a_1^*$  and  $t_2^*$  antibonding orbitals. An arctangent step function representing the transition of ejected photoelectrons to the continuum has also been fitted to the spectrum. A

TABLE I. Peak positions, widths, and intensities of phosphates from least-squares fitting.

| Samples                                           | Peak positions ( $\pm 0.07$ eV) |          |          |          | Peak widths ( $\pm 0.01$ eV) |          |          |          | Intensities <sup>a</sup> ( $\pm 6\%$ ) |          |
|---------------------------------------------------|---------------------------------|----------|----------|----------|------------------------------|----------|----------|----------|----------------------------------------|----------|
|                                                   | <i>a</i>                        | <i>b</i> | <i>c</i> | <i>d</i> | <i>a</i>                     | <i>b</i> | <i>c</i> | <i>d</i> | <i>a</i>                               | <i>b</i> |
| Na <sub>3</sub> P <sub>3</sub> O <sub>7</sub>     | 134.55                          | 135.35   | 138.94   | 146.43   | 0.57                         | 0.57     | 3.50     | 4.29     | 0.029                                  | 0.017    |
| Na <sub>4</sub> P <sub>2</sub> O <sub>7</sub>     | 134.93                          | 135.83   | 138.20   | 146.37   | 0.45                         | 0.45     | 2.85     | 3.74     | 0.040                                  | 0.031    |
| Na <sub>5</sub> P <sub>3</sub> O <sub>7</sub>     | 135.13                          | 135.96   | 137.92   | 146.43   | 0.56                         | 0.56     | 3.14     | 3.71     | 0.050                                  | 0.031    |
| Na <sub>7</sub> P <sub>5</sub> O <sub>16</sub>    | 135.43                          | 136.33   | 138.02   | 146.40   | 0.62                         | 0.62     | 2.87     | 3.48     | 0.079                                  | 0.067    |
| Na <sub>20</sub> P <sub>18</sub> O <sub>55</sub>  | 135.45                          | 136.31   | 137.94   | 146.36   | 0.58                         | 0.58     | 2.78     | 3.25     | 0.134                                  | 0.110    |
| Na <sub>30</sub> P <sub>28</sub> O <sub>85</sub>  | 135.46                          | 136.33   | 137.97   | 146.36   | 0.61                         | 0.61     | 2.78     | 3.30     | 0.151                                  | 0.139    |
| Na <sub>46</sub> P <sub>44</sub> O <sub>133</sub> | 135.42                          | 136.30   | 137.77   | 146.36   | 0.58                         | 0.58     | 2.83     | 3.23     | 0.154                                  | 0.128    |
| Na <sub>93</sub> P <sub>91</sub> O <sub>274</sub> | 135.51                          | 136.38   | 137.85   | 146.44   | 0.58                         | 0.58     | 2.82     | 3.38     | 0.163                                  | 0.136    |

<sup>a</sup>The intensities are normalized to peak (*c*).

number of conditions and constraints were introduced to obtain meaningful fits. First, the position of the arctangent step function was aligned just before peak *c*. This position is preceded by excitonic states (peaks *a* and *b*) which are observed in certain solids and generally lie below the bottom of the conduction band (continuum).<sup>26</sup> Second, the peak widths of peaks *a* and *b* (the spin-orbit

doublet) were constrained to be equal. All peak heights and peak positions were allowed to vary. Except for peaks *a* and *b*, the widths of the other peaks were allowed to vary.

Three XANES spectra of polyphosphate, fitted as described above, are shown in Figs. 5(A)–5(C). All peak positions, peak widths, relative intensities (normalized to peak *c*) are summarized in Table I. Figure 6 shows the positions of peaks *a* and *b* as a function of *n*. From Fig. 6 and Table I we find that the peak *a* position shifts to high energy when chain length increases from PO<sub>4</sub><sup>3-</sup> (*n*=1), to P<sub>5</sub>O<sub>16</sub><sup>7-</sup> (*n*=5). There is no obvious increase in energy above *n*=5. The same trend has been found in XPS studies of sodium phosphate glasses.<sup>19,48</sup> This is expected, since the difference between XPS and XANES is in the final state of the ejected electron from the 2*p* core level. Since changes in screening affects the inner shells more than the unoccupied levels, shifts observed in XANES

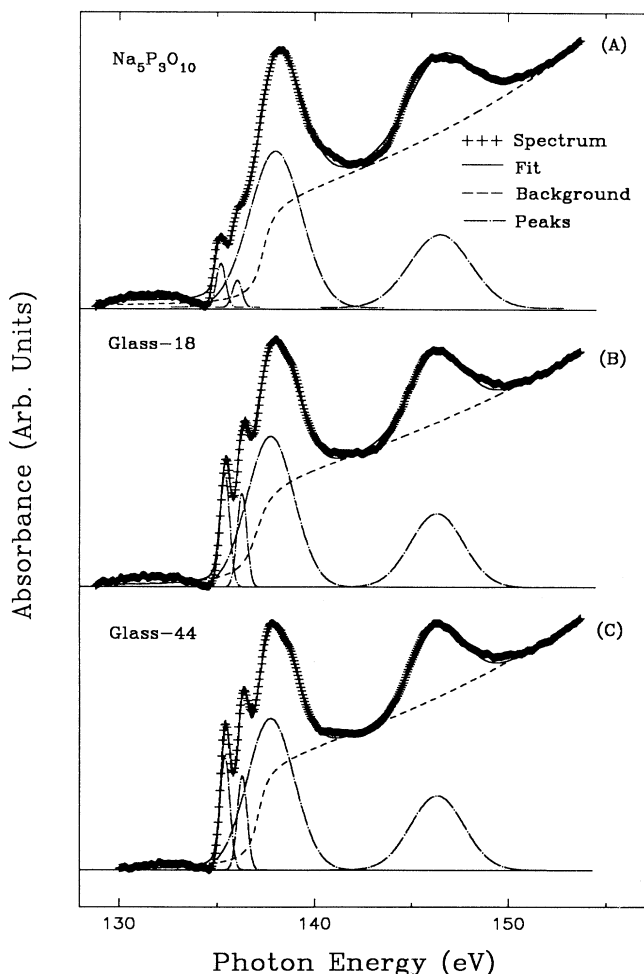


FIG. 5. The least-squares fitting of polyphosphate spectra: (A) Na<sub>5</sub>P<sub>3</sub>O<sub>10</sub>; (B) Na<sub>20</sub>P<sub>18</sub>O<sub>55</sub>; (C) Na<sub>46</sub>P<sub>44</sub>O<sub>133</sub>.

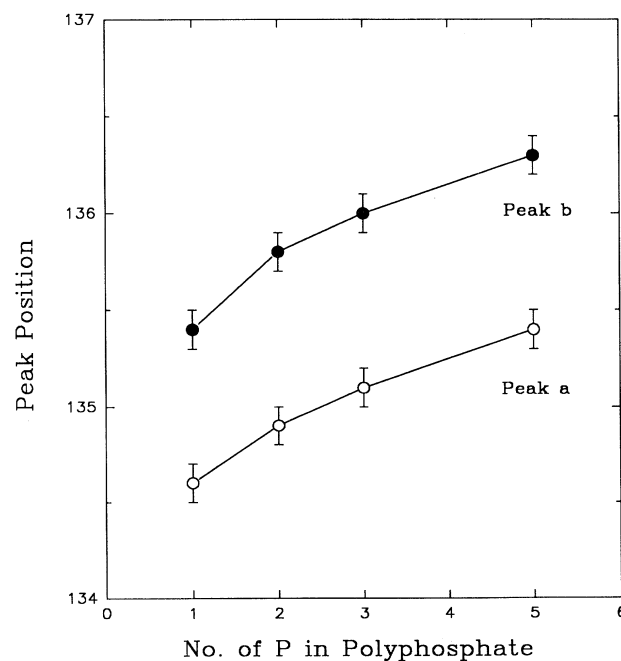


FIG. 6. A plot of the pre-edge doublet peak positions against the number of P in polyphosphates (chain length).

and XPS are generally similar. However, the XPS peak widths are at least 1.5 eV compared to the 0.6 eV observed in our spectra. In XPS it has been found that the P  $2p$ ,  $2s$ , and O  $1s$  binding energies are proportional to chain length.<sup>19</sup> This has been attributed to the fact that as the chain length increases, more bridging oxygen forms, and thus the electron density around O is reduced, which makes the core electrons more tightly bound. Also from Table I, we find that the peak position of peak  $d$  in all the spectra remains constant at 146.4 eV.

The chain length versus the relative area of peak  $a$  is plotted in Fig. 7. In order to compare the peak areas, the peak intensities of peaks  $a$  and  $b$  have been normalized to peak  $c$ . It is obvious from Fig. 7 that the ratio  $a:c$  increases sharply from  $\text{PO}_4^{3-}$  ( $n=1$ ) to  $\text{P}_{18}\text{O}_{55}^{17-}$  ( $n=18$ ), then levels off relatively for higher polyphosphates. It is very interesting that the plot in Fig. 7 is very similar to what we found in Fig. 2.

Now, using Table I and Fig. 7 we can directly determine the number of P in sodium polyphosphate glasses. The relative error for area measurement was estimated at about 6% from the standard deviation from duplicate spectra. As we noticed in the figure, up to  $n=18$ , the change of the number of phosphorus versus the peak area is large and as a result chain length can be determined with good accuracy. Above  $n=18$ , the change is rather subtle and thus the result will be less accurate. This intensity measurement is much more sensitive than the use of chemical shift shown in Fig. 6. There, the change in the peak position versus the chain length is small and can only be used up to  $p=5$ . This technique is also much more sensitive than XPS, because the peak widths in the XPS spectra are much larger than those in the XANES spectra (1.5 vs 0.6 eV). However, it should be pointed out that polyphosphate constitutes a range of polyphosphates. Therefore the method is a semiquantitative one and we may obtain an average chain length in an unknown phosphate system. The major advantage of this method is that it can be applied to thin films and surfaces

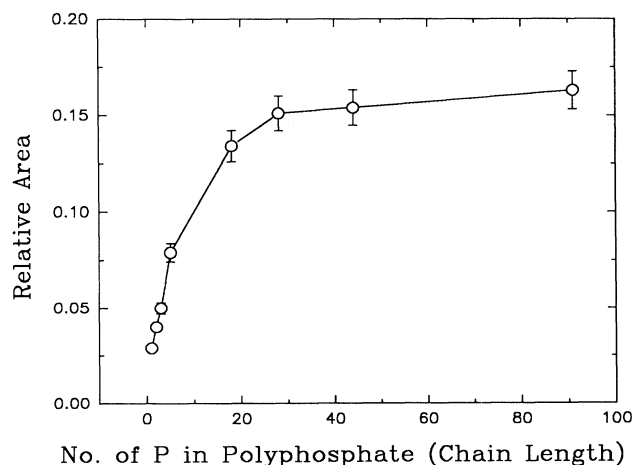


FIG. 7. Number of P in polyphosphates (chain length) as a function of relative area of peak  $a$ .

where other techniques such as titration and liquid chromatography cannot be utilized. The P  $L$ -edge XANES is used here semiquantitatively to solve such a complex problem. This will have very important application in systems such as surface films. For example, the results of this investigation have been applied to characterize the nature of polyphosphate in tribochemical films.<sup>38,49</sup>

#### P $K$ -edge EXAFS spectra of polyphosphates

Since the spectral pattern in the  $K$ -edge XANES of phosphate glasses does not change substantially, the information gained cannot be used to fingerprint the phosphate chain length. However, the analysis of  $K$ -edge spectra in the range of 50–1000 eV above the ionization threshold, or EXAFS region, can be used to estimate the bond distance and the coordination number around the absorbing atom.

Figure 8 shows a typical x-ray-absorption spectrum recorded to  $\sim 600$  eV above the P  $K$ -edge for  $\text{NaH}_2\text{PO}_4$ . A standard procedure has been used to extract the bond distance and coordination number from the experimental x-ray-absorption spectra.<sup>50</sup> The EXAFS interference function is defined by  $\chi(k)=[\mu(E)-\mu_0(E)]/\mu_0(E)$ , where  $E$  and  $k$  are the x-ray photon energy and the wave number of the photoelectron ejected by the x-ray photon, respectively. The coefficient  $\mu(E)$  refers to absorption by an atom in the material of interest, while  $\mu_0(E)$  refers to absorption by an atom in the free state, both of which are a function of  $k$ . In order to relate  $\chi(k)$  to structural parameters, it is necessary to convert  $E$  into the photoelectron wave vector  $k$  by the relationship

$$k = [2m/\hbar^2(E - E_0)]^{1/2}, \quad (2)$$

where  $m$  is the mass of the electron,  $\hbar$  is Planck's constant divided by  $2\pi$ , and  $E_0$  is the threshold energy of the absorption edge. In our experiment, the  $E_0$  was determined from the inflection point at the absorption threshold. The transformation of  $\chi(E)$  into  $\chi(k)$  in  $k$  space gives rise to

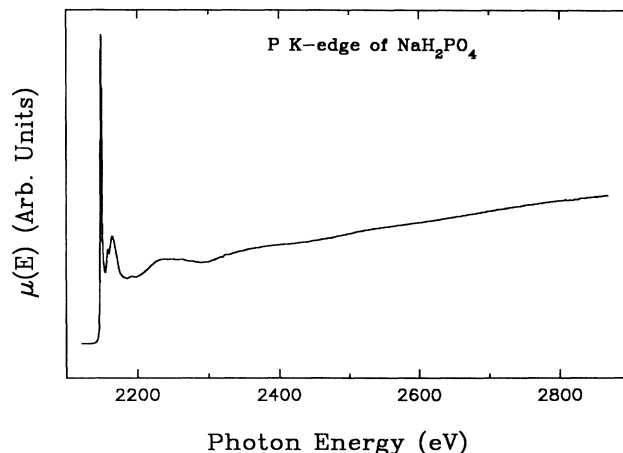


FIG. 8. P  $K$ -edge spectrum of  $\text{NaH}_2\text{PO}_4$ .

$$\chi(k) = \sum N_j F_j(k) / (kr_j^2) \exp(-2\sigma_j^2 k^2) \times \exp(-2r_j/\lambda) \sin[2kr_j + \phi_j(k)], \quad (3)$$

where  $F_j(k)$  is the backscattering amplitude from each of the  $N_j$  neighboring atom of type  $j$ ,  $\sigma_j$  is the Debye-Waller factor which accounts for thermal vibration and possible statistical disorder, viz., distribution of distances,  $r_j$  is the mean internuclear distance between the central (absorbing) atom and atoms in the  $j$ th neighbor shell,  $\lambda$  is the mean free path of the photoelectron due to the finite core-hole lifetime and interactions with the valence electrons,  $\phi_j(k)$  is the scattering phase shift due to both the center and backscattering atom, and  $k$  is related to the experimental wave number of the photoelectron.

In practice, the  $\chi(k)$  of phosphates were extracted from the raw absorption data (Fig. 8) in following steps. First, the raw data was truncated above the edge to exclude the XANES region and a pre-edge background is removed. A computer program<sup>51</sup> was used to convert the photoelectron energy scale to  $k$  space using the above equation. At this stage,  $\chi(k)$  was multiplied by  $k^3$  to enhance features at high  $k$  values. Second, EXAFS  $k^3\chi(k)$  was obtained by subtracting post-edge background function  $\mu_0(k)$ . This background is approximately the smooth part of  $\mu(k)$  and generated by fitting  $\mu(k)$  to a multisection polynomial spline function of 3–4 sections. Finally the data were normalized by the edge jump obtained by extrapolation of a straight line fit above the edge.

The  $k^3\chi(k)$  versus  $k$  is plotted for orthophosphate and polyphosphate glasses in Figs. 9(A)–9(C). As is noticed from the spectra, the amplitude and positions for the three spectra are very similar. This indicates that the coordination number and bond distances for the three samples should be very similar. In order to obtain a more quantitative picture, the  $k^3\chi(k)$  was Fourier transformed in  $R$  space. The magnitude of the corresponding Fourier transform of the P EXAFS are shown in Figs. 9(D)–9(F).

This gives a qualitative picture of the local structure around P. Since the transform is made without including the phase shift, all of the peaks in  $F(R)$  are shifted closer to the origin. Further data analyses are needed in order to obtain quantitative structural information about the local environment of the absorbing atom.

In general, the parameters (distance  $R$ , coordination number  $N$ , and relative mean square disorder  $\sigma_j^2$ ) relevant to a particular structure model can be deduced from the Fourier-filtered experimental EXAFS. This is achieved by reverse Fourier transform (RFT). The RFT (shell by shell) permits a well-defined phase and amplitude function to be determined for each shell distinguishable in the  $F(R)$  function. In order to obtain the structural parameters from the phase and amplitude function, the scattering phase shift and amplitude scale needs to be corrected and calibrated respectively. Thus model phase or amplitudes, either calculated or derived experimentally, are needed. In this paper, two calculated tables called FEFF<sup>52</sup> and McKale<sup>53</sup> have been used. The phase shift and amplitude of  $\text{NaH}_2\text{PO}_4$  was used as experimental model for glass analysis.

The main peak [see Fig. 9(D)] around 1.2 Å in the Fourier transform is assigned to the first P-O coordination shell. Several small peaks in the higher distance are likely due to high-frequency noise. A symmetric Hanning window was chosen for reverse Fourier transform [Fig. 9(D), dashed line]. Then utilizing the calculated (FEFF and McKale) phase shift and amplitude function, P-O distance  $R$  and coordination number  $N$  have been determined. These results are summarized in Table II. The P-O bond distance of  $\text{NaH}_2\text{PO}_4$  derived from EXAFS, using FEFF or using McKale, is very close to the diffraction data of 1.56 Å.<sup>54</sup> As is expected from the structure of the compound, the coordination number  $N$  is essentially 4 (3.9 and 3.6, respectively, from FEFF and McKale). Having measured the phase shift and amplitude for a known structure, we can use them for the analysis of the polyphosphate glasses.

Two glass samples have been analyzed using the same

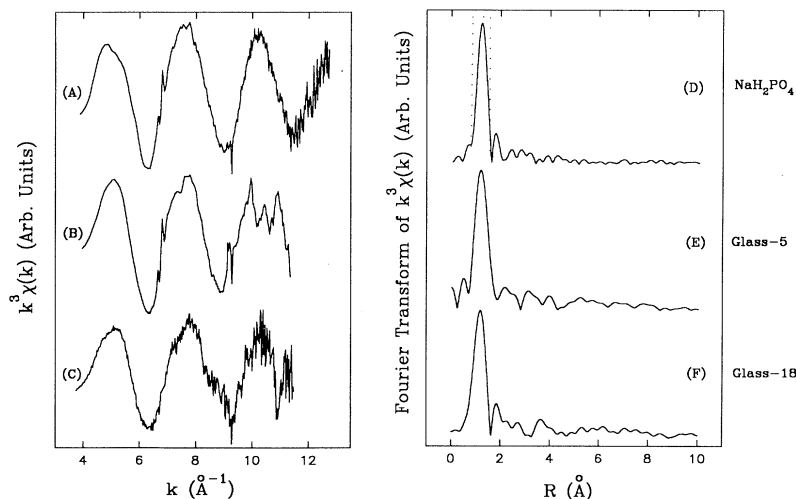


FIG. 9. EXAFS spectra (left) and their Fourier transform spectra (right) of three phosphates: (A) and (D)  $\text{NaH}_2\text{PO}_4$ ; (B) and (E)  $\text{Na}_7\text{P}_5\text{O}_{16}$ ; (C) and (F)  $\text{Na}_{20}\text{P}_{18}\text{O}_{55}$ .

TABLE II. EXAFS data analysis.

| Compounds                                                    | P-O bond distance (Å) |        |                    | Coordination number |        |       | Diffraction data of P-O |
|--------------------------------------------------------------|-----------------------|--------|--------------------|---------------------|--------|-------|-------------------------|
|                                                              | FEFF                  | McKale | Expt. <sup>a</sup> | FEFF                | McKale | Expt. |                         |
| NaH <sub>2</sub> PO <sub>4</sub>                             | 1.55                  | 1.54   |                    | 3.9                 | 3.6    |       | 1.56 <sup>b</sup>       |
| Glass-5 (Na <sub>7</sub> P <sub>5</sub> O <sub>16</sub> )    | 1.55                  | 1.54   | 1.54               | 3.6                 | 3.3    | 4.8   |                         |
| Glass-18 (Na <sub>20</sub> P <sub>18</sub> O <sub>55</sub> ) | 1.55                  | 1.53   | 1.55               | 3.7                 | 3.3    | 5.0   |                         |

<sup>a</sup>The phase shift and amplitude of NaH<sub>2</sub>PO<sub>4</sub> were used for the glasses.

<sup>b</sup>Diffraction data from KH<sub>2</sub>PO<sub>4</sub>.

procedure described for sodium dihydrogen orthophosphate. Their  $k^3$ -weighted P *K*-edge EXAFS are shown in Figs. 9(B) and 9(C), and the magnitude of their Fourier transforms is shown in Figs. 9(E) and 9(F). Again, a single coordination shell is observed for these glasses in the Fourier transform plots around 1.2 Å. The weak peaks should have the same origin (probably noise) as those of the model compound. Comparing *R* and *N* of the glasses with those of NaH<sub>2</sub>PO<sub>4</sub> in Table II, we notice that the chemical environment of P in these two glasses looks very similar to that of NaH<sub>2</sub>PO<sub>4</sub>. That means P in the glasses is coordinated to four oxygen atoms and the average P-O bond distance is about 1.55 Å. The bond distances and coordination numbers extracted from EXAFS results accounts for an average value. As the chain length increases in polyphosphates, the number of bridging P-O bonds also increases. The P-O bridging distance is 1.60 Å,<sup>55</sup> which is longer than the terminal P-O. Since the error in EXAFS measurements is expected to be 0.02 Å, the small changes in the bond distances cannot be detected in the EXAFS. Thus we are not able to deduce the chain length of the polyphosphate glasses from the EXAFS data using the P-O bond distance and coordination number.

## CONCLUSIONS

From the above discussion the following conclusions can be drawn:

(1) Both the P *K*-edge and *L*-edge XANES are very sensitive to the electron charge density around the absorbing atom. The P *K* and *L* edges shift to higher energy as the core level becomes less screened by the ligand surrounding the absorbing atom. The fine features in the spectra have been assigned to electronic transitions from the P core levels to appropriate antibonding orbitals

below and above the edge.

(2) While the P *K*-edge XANES can provide limited structural information, the P *L* edge is very sensitive to the small local structural changes caused by bridging P-O bonds in polyphosphates.

(3) Using the ratio of intensities from the P *L*-edge XANES spectra of the polyphosphates, it was possible to construct a calibration curve for chain length determination. It was found that the chain length was proportional to the intensity of the first sharp peaks in the XANES spectra of the polyphosphates. This calibration plot will be very useful for determining the phosphate chain length in thin films and biological molecules where other techniques cannot be applied. An important objective of XANES spectroscopy is to provide nondestructive and quantitative results, in complex systems. The P *L*-edge XANES is applied semiquantitatively to solve such a complex problem.

(4) Bond distances and the coordination numbers obtained, analyzing the EXAFS region of the absorption spectra, indicated that the small changes in the bond distance, going from orthophosphate to polyphosphates cannot be detected by the EXAFS analysis.

## ACKNOWLEDGMENTS

This study was financially supported by a grant from the Ontario Centre for Materials Research (OCMR), University Research Incentive Fund (URIF) of Ontario, Imperial Oil (Esso) of Canada, the National Research Council of Canada, and the Natural Science and Engineering Research Council of Canada. We are grateful to Dr. Kim Fyfe from the Imperial Oil (Esso) for her continued support, staff of the Synchrotron Radiation Centre (SAC), University of Wisconsin, Madison, for their technical support, and NSF for supporting the SAC.

\*Author to whom correspondence should be addressed.

<sup>1</sup>J. R. Van Wazer, *Phosphorus and Its Compounds, Vol. 1: Chemistry* (Interscience, New York, 1958), p. 419.

<sup>2</sup>J. R. Van Wazer, *Phosphorus and Its Compounds, Vol. 1: Chemistry* (Ref. 1), p. 421.

<sup>3</sup>R. K. Brow, R. K. Kirkpatrick, and G. L. Turner, *J. Non-Cryst. Solids* **116**, 39 (1990).

<sup>4</sup>G. Wignall, R. Rotheron, G. Longman, and G. Woodward, *J. Mater. Sci.* **12**, 1039 (1977).

<sup>5</sup>(a) B. C. Sales and L. A. Boatner, *Science* **226**, 45 (1984); (b)

*Mater. Lett.* **2**, 301 (1984).

<sup>6</sup>(a) P. Benassi, A. Fontana, and P. A. M. Rodrigues, *Phys. Rev. B* **43**, 1756 (1991); (b) P. A. M. Rodrigues, P. Benassi, and A. Fontana, *J. Non-Cryst. Solids* **143**, 274 (1992).

<sup>7</sup>(a) P. Losso, B. Schnabel, C. Jäger, U. Sternberg, D. Stachel, and D. O. Smith, *J. Non-Cryst. Solids* **143**, 265 (1992); (b) E. C. Onyiriuka, *J. Non-Cryst. Solids* **163**, 268 (1993).

<sup>8</sup>M. Ashizuka and T. Sakai, *Yogyo Kyokai Shi* **91**, 87 (1983).

<sup>9</sup>E. Kordes and J. Navarrete, *Glastechn. Ber.* **46**, 113 (1973).

<sup>10</sup>L. D. Bogomolova, V. A. Tachkin, V. W. Lazukin, T. K.

- Pavlushkina, and V. A. Shmuckler, *J. Non-Cryst. Solids* **28**, 375 (1978).
- <sup>11</sup>H. Hosono, H. Kawazoe, and T. Kawazawa, *J. Non-Cryst. Solids* **37**, 427 (1980).
- <sup>12</sup>E. Masubara, Y. Waseda, M. Ashizuka, and E. Ishida, *J. Non-Cryst. Solids* **103**, 117 (1988).
- <sup>13</sup>W. Matz, D. Stachel, and E. A. Goremychkin, *J. Non-Cryst. Solids* **101**, 80 (1988).
- <sup>14</sup>(a) B. N. Nelson and G. J. Exarhos, *J. Chem. Phys.* **71**, 2739 (1979); (b) T. Minami, T. Katsuda, and M. Tanaka, *J. Phys. Chem.* **83**, 1306 (1979); (c) J. J. Hudgens and S. W. Martin, *J. Am. Ceram. Soc.* **76**, 1691 (1993); (d) D. E. C. Corbridge and E. J. Lowe, *J. Chem. Soc.* p. 493 (1954).
- <sup>15</sup>B. C. Sales, R. S. Ramsey, J. B. Bates, and L. A. Boatner, *J. Non-Cryst. Solids* **87**, 137 (1986).
- <sup>16</sup>A. Paul, *Chemistry of Glasses* (Chapman and Hall, New York, 1982), p. 204.
- <sup>17</sup>D. L. Griscom, *J. Non-Cryst. Solids* **40**, 211 (1980).
- <sup>18</sup>R. K. Sato, R. J. Kirkpatrick, and R. K. Brow, *J. Non-Cryst. Solids* **143**, 257 (1992).
- <sup>19</sup>R. Gresch, W. Müller-Warmuth, and H. Dutz, *J. Non-Cryst. Solids* **34**, 127 (1979).
- <sup>20</sup>E. Brückner, H.-U. Chun, H. Goretzki, and M. Sammet, *J. Non-Cryst. Solids* **42**, 49 (1980).
- <sup>21</sup>(a) J. E. Harries, D. W. L. Hukins, C. Holt, and S. S. Hasnain, *J. Phys. C* **19**, 6859 (1986); (b) J. E. Harries, D. W. L. Hukins, C. Holt, and S. S. Hasnain, *J. Cryst. Growth* **84**, 563 (1987); (c) L. S. Nelson, Jr., C. Holt, J. E. Harries, and D. W. L. Hukins, *Physica B* **158**, 105 (1989); (d) N. Sato and T. Minami, *J. Mater. Sci.* **24**, 4419 (1989).
- <sup>22</sup>E. J. Griffith, *J. Am. Chem. Soc.* **79**, 509 (1957).
- <sup>23</sup>G. M. Bancroft, *Can. Chem. News* **44**, 15 (1992).
- <sup>24</sup>M. Kasrai, Z. Yin, G. M. Bancroft, and K. H. Tan, *J. Vac. Sci. Technol. A* **11**, 2694 (1993).
- <sup>25</sup>*X-ray Absorption: Principles, Applications, Techniques of EXAFS, SEXAFS and XANES*, edited by D. C. Koningsberger and R. Prins (Wiley, New York, 1988).
- <sup>26</sup>J. Stöhr, in *NEXAFS Spectroscopy*, Springer Series in Surface Science, edited by R. Gomer (Springer, New York, 1992), Vol. 25.
- <sup>27</sup>D. G. L. Sutherland, M. Kasrai, G. M. Bancroft, Z. F. Liu, and K. H. Tan, *Phys. Rev. B* **48**, 14989 (1993).
- <sup>28</sup>G. P. Huffman, S. Mitra, F. E. Huggins, N. Shah, S. Vaidya, and F. Lu, *Energy Fuel* **5**, 574 (1991).
- <sup>29</sup>M. Kasrai, J. R. Brown, G. M. Bancroft, K. H. Tan, and J. M. Chen, *Fuel* **69**, 411 (1990).
- <sup>30</sup>S. Bodeur, I. Nenner, and P. Millie, *Phys. Rev. A* **34**, 2986 (1986).
- <sup>31</sup>T. A. Ferrett, M. N. Piancastelli, D. W. Lindle, P. A. Heimann, and D. A. Shirley, *Phys. Rev. A* **38**, 701 (1988).
- <sup>32</sup>R. G. Cavell and K. H. Tan, *Chem. Phys. Lett.* **197**, 161 (1992).
- <sup>33</sup>J. S. Tse, Z. F. Liu, J. D. Bozek, and G. M. Bancroft, *Phys. Rev. A* **34**, 2986 (1989).
- <sup>34</sup>J. D. Bozek, G. M. Bancroft, and K. H. Tan, *Chem. Phys.* **145**, 131 (1990).
- <sup>35</sup>(a) W. H. E. Schwarz and R. J. Buenker, *Chem. Phys.* **13**, 153 (1976); (b) W. H. E. Schwarz, *ibid.* **11**, 217 (1975).
- <sup>36</sup>P. L. Hansen, R. Brydson, and D. W. McComb, *Microsc. Microanal. Microstruct.* **3**, 213 (1992).
- <sup>37</sup>J. L. Dehmer, *J. Chem. Phys.* **56**, 4496 (1972).
- <sup>38</sup>Z. Yin, M. Kasrai, G. M. Bancroft, K. F. Laycock, and K. H. Tan, *Tribol. Int.* **26**, 383 (1993).
- <sup>39</sup>J. R. Van Wazer and K. A. Hoist, *J. Am. Chem. Soc.* **72**, 639 (1950).
- <sup>40</sup>U. P. Strauss, E. H. Smith, and P. L. Wineman, *J. Am. Chem. Soc.* **75**, 3935 (1953).
- <sup>41</sup>R. Pfanstiel and R. K. Iler, *J. Am. Chem. Soc.* **74**, 6062 (1952).
- <sup>42</sup>U. P. Strauss and T. L. Treitler, *J. Am. Chem. Soc.* **77**, 1473 (1955).
- <sup>43</sup>U. P. Strauss and T. L. Treitler, *J. Am. Chem. Soc.* **78**, 3553 (1956).
- <sup>44</sup>J. R. Van Wazer, *Phosphorus and Its Compounds, Vol. 1: Chemistry* (Ref. 1), p. 439.
- <sup>45</sup>J. R. Van Wazer, *J. Am. Chem. Soc.* **72**, 644 (1950).
- <sup>46</sup>I. Gutsov, in *The Structure of Glasses*, edited by E. A. Porai-Kishits (Consultants Bureau, New York, 1966), Vol. 7, p. 154.
- <sup>47</sup>M. Kasrai, M. Fuller, M. Scaini, Z. Yin, R. W. Brunner, G. M. Bancroft, M. E. Fleet, K. Fyfe, and K. H. Tan, in *Proceedings of the 21st Leeds-Lyon Symposium on Tribology*, Leeds, England, September 1994, edited by D. Dowson (Elsevier, Amsterdam, in press).
- <sup>48</sup>E. Fluck and D. Weber, *Pure Appl. Chem.* **44**, 373 (1975).
- <sup>49</sup>Z. Yin, M. Kasrai, G. M. Bancroft, K. Fyfe, and K. H. Tan (unpublished).
- <sup>50</sup>(a) F. W. Lytle, D. E. Sayers, and E. A. Stern, *Phys. Rev. B* **11**, 4825 (1975); (b) P. A. Lee, P. H. Citrin, P. Eisenberger, and B. M. Kinkaid, *Rev. Mod. Phys.* **53**, 769 (1981).
- <sup>51</sup>T. Tyliczszak (unpublished).
- <sup>52</sup>J. J. Rehr, J. de Leon, S. I. Zabinsky, and R. C. Albers, *J. Am. Chem. Soc.* **113**, 5135 (1991).
- <sup>53</sup>A. G. McKale, B. W. Veal, A. P. Paulikas, S.-K. Chan, and G. S. Knapp, *J. Am. Chem. Soc.* **110**, 3763 (1988).
- <sup>54</sup>B. C. Frazer and R. Pepinsky, *Acta Crystallogr.* **6**, 273 (1953).
- <sup>55</sup>D. W. J. Cruickshank, *Acta Crystallogr.* **17**, 6672 (1964).